8.2.4 Epidermal Growth Factor Receptor-Targeted Liposomes

Epidermal growth factor receptor (EGFR) tyrosine kinase plays a fundamental role in signal transduction pathways and the uncontrolled activation of this EGFR-mediated signaling may be due to overexpression of the receptors in numerous tumors. Kullberg and coworkers investigated EGF-conjugated PEGylated liposome delivery vehicle, containing water soluble boronated phenanthridine, WSP1, or water soluble boronated acridine, WSA1, for EGFR targeting. In the case of WSA1 a ligand dependent uptake was obtained and the boron uptake was as good as if free WSA1 was given. No ligand-dependent boron uptake was seen for WSP1-containing liposomes. *In vitro* boron uptake by glioma cells (6.29 ± 1.07 μg/g cells) was observed with WSA1-encapsulated EGF-
Q3 conjugated PEGylated liposomes (Kullberg et al., 2003)(Figure 8.3).

Cetuximab, a recombinant chimeric monoclonal antibody, binds to the extracellular domain of the EGFR, thereby preventing the activation and subsequent dimerization of the receptor. Lee and coworkers developed cetuximab-immunoliposomes as an alternative immunoliposome for targeting of EGFR(+) glioma cells through a cholesterol-based membrane anchor, maleimido-PEG-cholesterol (Mal-PEG-Chol), to conjugated cetuximab to liposomes. BSH-encapsulated cetuximab-immunoliposomes were evaluated for targeted delivery to human EGFR gene transfected $F98_{EGFR}$ glioma cells. Much greater (~8-fold) cellular uptake of boron was obtained using cetuximab-immunoliposomes in EGFR(+) $F98_{EGFR}$ compared with nontargeted human IgG-immunoliposomes (Pan, et al., 2007).

8.2.5 Transferrin Receptor-Targeted Liposomes

Transferrin (TF) receptor-mediated endocytosis is a normal physiological process by which TF delivers iron to the cells and higher concentration of TF receptor has been observed on most tumor cells in comparison with normal cells. Maruyama and coworkers developed TF-conjugated PEG liposome. This liposome showed a prolonged residence time in the circulation and low RES uptake in tumor-bearing mice, resulting in enhanced extravasation of the liposomes into the solid tumor tissue, where the liposomes were internalized into tumor cells by receptor-mediated endocytosis (Ishida et al., 2001). The TF-conjugated PEG liposomes and PEG liposomes encapsulating ^{10}BSH were prepared and their tissue distributions in Colon 26 tumor-bearing mice after *i.v.* injection were compared with those of bare liposomes and free ^{10}BSH. When TF-PEG liposomes were injected at a dose of 35 mg ^{10}B/kg, a prolonged residence time in the circulation and low uptake by the reticuloendothelial system (RES) were observed in Colon 26 tumor-bearing mice, resulting in enhanced accumulation of ^{10}B into the solid tumor tissue. TF-PEG liposomes maintained a high ^{10}B level in the tumor, with concentrations over 30 μg of boron per gram of tumor for at least 72 h after injection. On the other hand, the plasma level of ^{10}B decreased, resulting in a tumor/plasma ratio of 6.0 at 72 h after injection. Administration of ^{10}BSH encapsulated in TF-PEG liposomes at a dose of 5 or 20 mg ^{10}B/kg and irradiation with 2×10^{12} neutrons/cm^2 for 37 min produced tumor growth suppression and improved long-term survival compared with boron-loaded PEG liposomes and bare liposomes, and free ^{10}BSH. Masunaga and coworkers evaluated biodistribution of ^{10}BSH and $Na_2{}^{10}B_{10}H_{10}$-encapsulated TF-PEG liposomes in SCC VII tumor-bearing mice (Masunaga et al.,

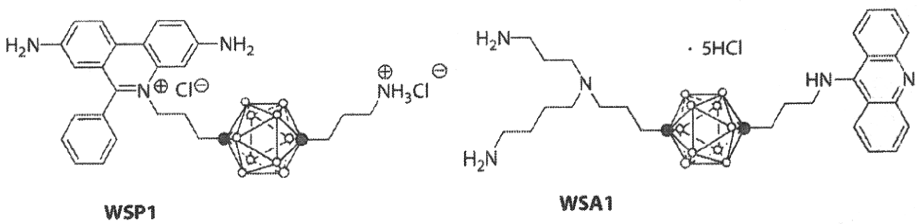

FIGURE 8.3 Structures of WSP1 and WSA1.

2006). The kinetics in the ^{10}B concentration in tumors loaded with both liposomes were similar except that ^{10}B concentrations were greater 24 h after the administration of $Na_2{}^{10}B_{10}H_{10}$ than ^{10}BSH in TF-PEG liposomes and ^{10}B concentration in tumors was 35.6 μg of boron per gram of tumor with injection of $Na_2{}^{10}B_{10}H_{10}$-encapsulated TF-PEG liposomes via the tail vein at a dose of 35 mg ^{10}B/kg. Q4

8.3 BORON LIPID–LIPOSOME APPROACH

Since a demonstration of liposomes as models for the biomembrane mimics were reported by Bangham (Bangham et al., 1965) and a first totally synthetic bilayer vesicle of didodecacyldimethylammonium bromide by Kunitake (Kunitake 1992; Kunitake et al., 1977), various self-organization bilayer membranes have been synthesized (Menger et al., 1995). Generally, amphiphiles of liposomal membranes consist of a long hydrocarbon chain, which is called a tail, and a hydrophilic part (Allen, 1998; Maruyama, 2000); (Torchilin et al., 2002); (Betageri et al., 1993). In the meanwhile, development of lipophilic boron compounds embedded within the liposome bilayer, provides an attractive method to increase the overall efficiency of incorporation of boron-containing species, as well as raise the gross boron content of the liposomes in the formulation. Various boron lipids have been developed recently and those are classified into two groups: *nido*-carborane conjugates (**1**–**3**) and *closo*-dodecaborane conjugates (**4**–**11**) as shown in Figures 8.4 and 8.5, respectively. Less toxicity has been observed in the boron lipids belonging to the latter group. Q5 Q6 Q7

8.3.1 *NIDO*-CARBORANE AMPHIPHILE

Hawthorne and coworkers first introduced *nido*-carborane as a hydrophilic moiety into the amphiphile and this single-tailed *nido*-carborane amphiphile was utilized for liposomal boron delivery using tumor-bearing mice (Feakes et al., 1995; Watson-Clark et al., 1998). They synthesized the *nido*-carborane amphiphile **1** (Figure 8.4) from the reaction of decaborane and 1-octadecyne followed by degradation of the resulting carborane cage under basic conditions. Boronated liposomes were prepared from DSPC, cholesterol, and **1**. After the injection of liposomal suspensions in BALB/c mice bearing EMT6 mammary adenocarcinomas, the time-course biodistribution of boron was examined. At the low injected doses normally used (5–10 mg ^{10}B/kg), peak tumor boron concentrations of 35 μg of boron per gram of tumor and tumor/blood boron ratios of approximately

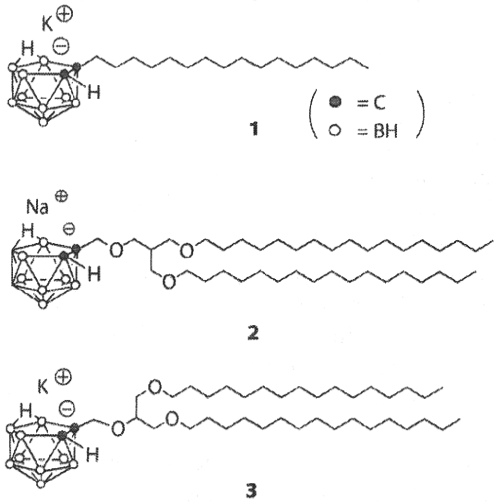

FIGURE 8.4 Structures of *nido*-carborane amphiphile and lipids.

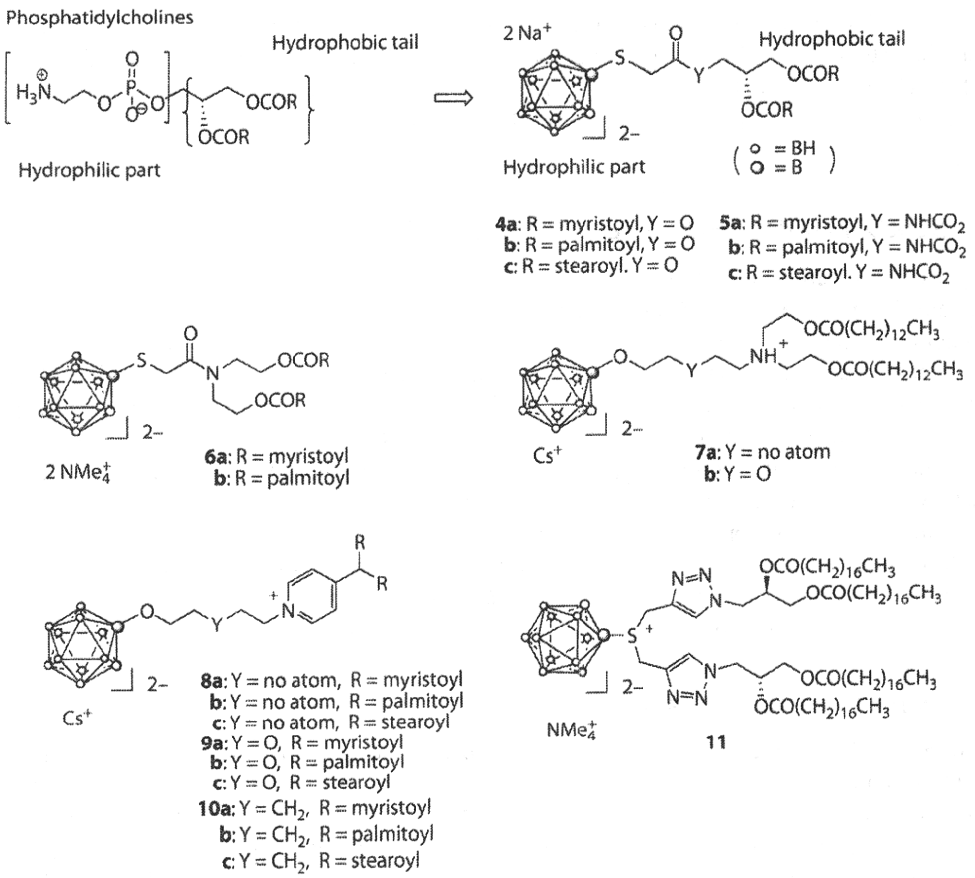

FIGURE 8.5 Structures of phosphatidylcholine and *closo*-dodecaborane lipids.

8 were achieved. These values are sufficiently high for the successful application of BNCT. The incorporation of both **1** and the hydrophilic species, $Na_3[1\text{-}(2'\text{-}B_{10}H_9)\text{-}2\text{-}NH_3B_{10}H_8]$, within the same liposome demonstrated significantly enhanced biodistribution characteristics, exemplified by maximum tumor boron concentration of 50 μg of boron per gram of tumor and tumor/blood boron ratio of 6.

8.3.2 *NIDO*-CARBORANE LIPIDS

Nakamura and coworkers developed *nido*-carborane lipid **2**, which consists of the *nido*-carborane moiety as the hydrophilic functionality conjugated with two long alkyl chains as the lipophilic functionality. Chemical synthesis of *nido*-carborane lipid **2** is shown in Scheme 8.1. Reaction of two equivalents of heptadecanol with 3-chloro-2-chloromethyl-1-propene using NaH as base gave the diether **12** in 93% yield and the hydroboration of **12** gave the corresponding alcohol **13** in 71% yield. The alcohol **13** was converted into the propargyl ether **14** in 48% yield by the treatment with propargyl bromide and the decaborane coupling of **6** was carried out in the presence of acetonitrile in toluene under reflux condition to give the corresponding *ortho*-carborane **15** in 80% yield. The degradation of the carborane cage by the treatment with sodium methoxide in methanol afforded the *nido*-carborane lipid **2** in 57% yield.

Analysis under a transmission electron microscope by negative staining with uranyl acetate showed stable vesicle formation of *nido*-carborane lipid **2**. The *nido*-carborane lipid **2** (CL) was incorporated into DSPC liposomes in a concentration-dependent manner (Nakamura et al., 2004).

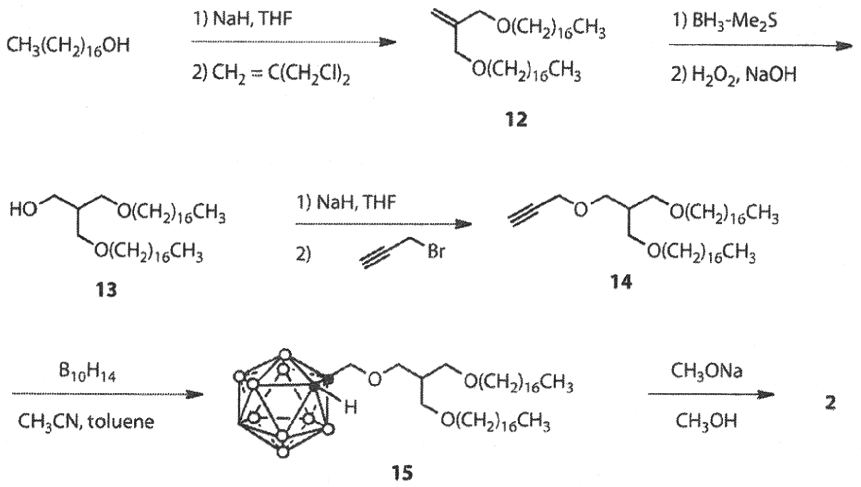

SCHEME 8.1 Synthesis of *nido*-carborane lipid **2** (CL).

Furthermore, TF could be introduced to the surface of *nido*-carborane lipid liposomes (Tf(+)-PEG-CL liposomes) by coupling TF to the PEG-CO_2H moieties of Tf(−)-PEG-CL liposomes. The biodistribution of Tf(+)-PEG-CL liposomes injected intravenously into colon 26 tumor bearing BALB/c mice revealed that Tf(+)-PEG-CL liposomes accumulated in tumor tissues and stayed there for a sufficiently long time to increase tumor/blood boron ratio, although Tf(-)-PEG-CL liposomes were gradually released from tumor tissues with time. A boron concentration of 22 μg of boron per gram of tumor was achieved by injecting Tf(+)-PEG-CL liposomes (7.2 mg ^{10}B/kg) into tumor-bearing mice. As noted earlier, BSH-encapsulated Tf(+)-PEG liposomes accumulated in tumors at 35.5 μg of boron per gram of tissue 72 h after administration of 35 mg ^{10}B/kg. Therefore, ^{10}B delivery to tumor tissues by Tf(+)-PEG-CL liposomes would be more efficient than that by BSH-encapsulated Tf(+)-PEG liposomes based on dose-dependent drug delivery efficacy. However, significant acute toxicity was observed in 50% of the mice when Tf(+)-PEG-CL liposomes were injected at a dose of 14 mg ^{10}B/kg. Injection of Tf(+)-PEG-CL liposomes at a dose of 7.2 mg ^{10}B/kg and irradiation with 2×10^{12} neutrons/cm^2 for 37 min at the KUR atomic reactor suppressed tumor growth and the average survival rate of mice not treated with Tf(+)-PEG-CL liposomes was 21 days, whereas that of treated mice was 31 days (Miyajima et al., 2006).

Hawthorne and coworkers also synthesized *nido*-carborane lipid **3** as shown in Scheme 8.2. The reaction of two equivalents of 1-hexadecanol with epichlorohydrin using sodium hydride gave the corresponding alcohol **16**. Propargylation of **16** followed by the decaborane coupling afforded the carborane **18**. Finally, degradation of the carborane cage of **18** proceeded in the presence of KOH in ethanol to give the *nido*-carborane lipid **3**.

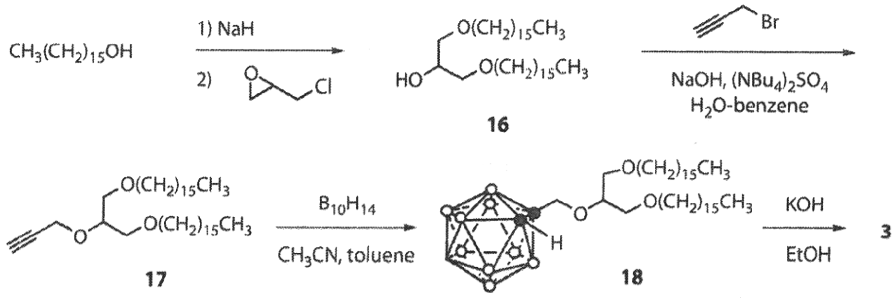

SCHEME 8.2 Synthesis of *nido*-carborane lipid **3**.

DSPC-free liposomes prepared from **3** and cholesterol exhibited a size distribution pattern of 40–60 nm, which was in the range normally associated with selective tumor uptake. Animal studies of the liposomes, containing **3**, DSPC, and cholesterol in varied proportions, were performed using male BALB/c mice (about 10 g body weight) bearing small EMT-6 tumors. Typically 200 μL of each liposome suspension was injected into the tail vein, and the behavior of the mice was followed for up to 48 h. Unfortunately, in each case, the liposomes were found to be very toxic: no mouse survived longer than 48 h following injection of doses ranging from 6 to 30 mg of boron per kg of body weight (Li et al., 2006).Due to the significant toxicity in both cases, *nido*-carborane framework is not suitable for use in BNCT.

8.3.3 *closo*-Dodecaborate Lipids

In order to solve the problem of the significant toxicity of liposomes prepared from *nido*-carborane lipids **2** and **3**, *closo*-dodecaborate has been focused on as an alternative hydrophilic function of boron lipids. BSH is known as a water-soluble divalent "*closo*-type" anion cluster and significantly lowered toxicity (Haritz et al., 1994), and thus has been utilized for clinical treatment of BNCT. Nakamura and coworkers succeeded in the synthesis of double-tailed *closo*-dodecaborate lipids **4a–c** and **5a–c**, which have a $B_{12}H_{11}S$-moiety as a hydrophilic function with chirality similar to natural phospholipids, such as distearoylphosphatidylcholine (DSPC), in their lipophilic tails (Lee et al., 2007; Nakamura et al., 2007a).

Synthesis of the hydrophobic tail functions of **22** is shown in Scheme 8.3. Reaction of the chiral alcohol **19** with 1.2 equivalents of bromoacetyl bromide gave the ester **20**, quantitatively, and the deprotection of **20** was carried out using catalytic amounts of *p*-TsOH in MeOH to give the corresponding diol **21**. Ester formation from diol **21** using various carboxylic acids was promoted by dicyclohexylcarbodiimide in the presence of catalytic amounts of *N,N*-dimethylaminopyridine in CH_2Cl_2 to afford the precursors **22a–c** in 61–75% yields. Synthesis of the hydrophobic tail functions of **27** is shown in Scheme 8.4. The chiral alcohol **19** was first protected with benzyl bromide using NaH and the resulting dioxolane **23** was converted into the diol **24** using aqueous AcOH in 83% yield. Ester formation of **24** using various carboxylic acids was carried out in a similar manner to give **25a–c**, quantitatively. Deprotection of the benzyl group of **25a–c** by hydrogenation gave the corresponding alcohols **26a–c** (89– > 99% yields), which then reacted with chloroacetyl isocyanate in CH_2Cl_2 to give **27a–c** in 74–98% yields.

Introduction of BSH into the hydrophobic tail functions **22** and **27** was examined using the "protected BSH (**28**)," which was prepared according to the Gabel's protocol (Gabel et al., 1993), as shown in Scheme 8.5. S-Alkylation of **28** with **22a–c** proceeded in acetonitrile at 70°C for 12–24 h, giving the corresponding *S*-dialkylated products **29**, which were immediately treated

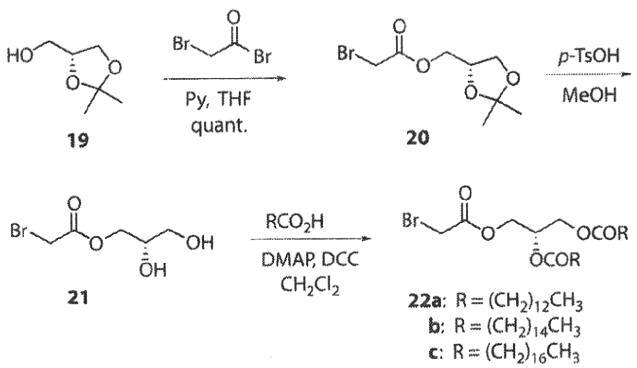

SCHEME 8.3 Synthesis of hydrophobic tail functions **22a–c**.

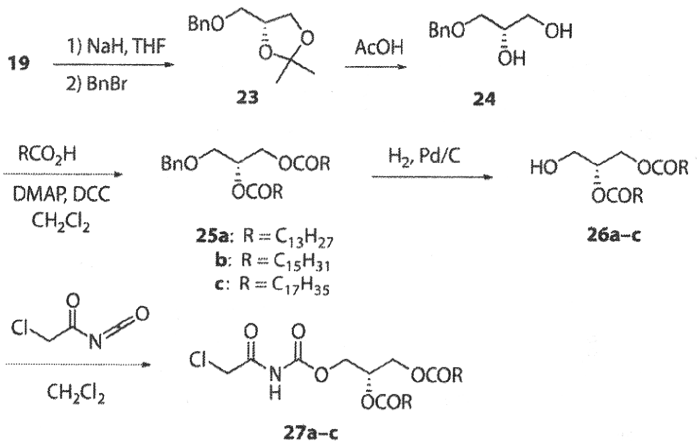

SCHEME 8.4 Synthesis of hydrophobic tail functions **27a–c**.

with tetramethylammonium hydroxide (1 equiv.) in acetone to give **4a–c** in 76–91% yields, as tetramethylammonium salts. In a similar manner, the **5a–c** were obtained from **27a–c** in 54–83% yields.

Calcein-encapsulation experiments revealed that the liposomes, prepared from boron cluster lipids **4**, DMPC, PEG-DSPE, and cholesterol, are stable at 37°C in FBS solution for 24 h.

The time-dependent biodistribution experiment of boronated liposomes prepared from closo-dodecaborate lipid **4c** and injected intravenously into colon 26 tumor bearing BALB/c mice (20 mg ^{10}B/kg) showed high ^{10}B accumulation in the tumor tissue (23 μg of boron per gram of tumor) 24 h after injection (Nakamura et al., 2009). In addition to determining ^{10}B concentration in various organs, neutron irradiation of the mice was carried out 24 h after administration of the boron liposomes in the JAEA atomic reactor (JRR-4). Tumor growth rate in mice administered with boron liposomes was significantly suppressed, although the administration of saline did not reduce tumor growth after neutron irradiation (Ueno et al., 2010).

Gabel and coworkers synthesized *closo*-dodecaborate lipids **6a** and **6b** as shown in Scheme 8.6. The introduction of the boron cluster was achieved by alkylation with "protected BSH (**28**)" and subsequent alkaline removal of the cyanoethyl protecting group (Gabel et al., 1993). In method A, 2 equivalents of the chloroanhydride of the fatty acids was allowed to react with diethanolamine. The resulting products *N,N*-(2-dimyristoyloxyethyl)- and *N,N*-(2-dipalmitoyloxyethyl)-amine (**30a** and **30b**, respectively) were reacted with chloroacetylchloride in the presence of triethylamine to obtain the chloroacetamides **31a** and **31b**. The reaction of **31a,b** and the tetramethylammonium salt of **28**

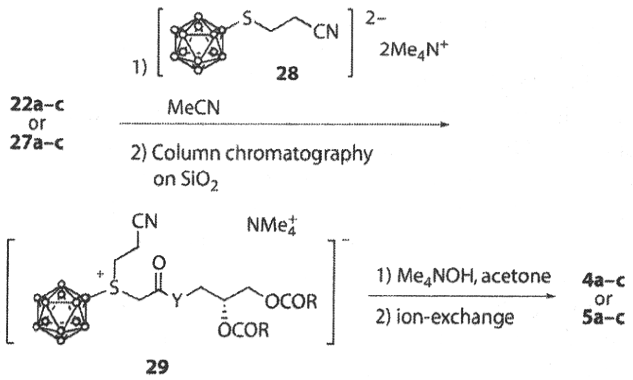

SCHEME 8.5 Synthesis of *closo*-dodecaborate lipids **4** and **5**.

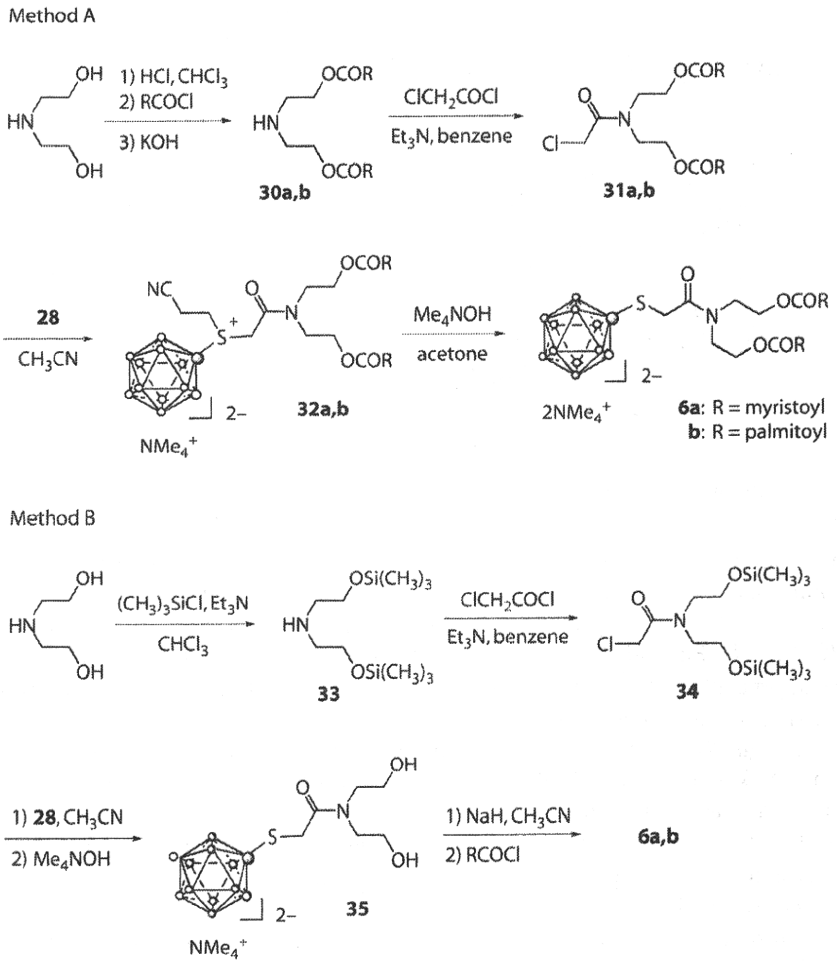

SCHEME 8.6 Synthesis of *closo*-dodecaborate lipids **6**.

produced sulfonium salts **32a,b**. The products **6a** and **6b** were obtained from the reaction of sulfonium salts **32a,b** with tetramethylammonium hydroxide in acetone. The yields of lipids **6a** and **6b** are 48–55% (overall yield from diethanolamine 25–28%).

The lipids were also able to be obtained through method B (Scheme 8.6). Two equivalents of chlorotrimethylsilane were reacted with diethanolamine in the presence of triethylamine. The resulting trimethylsilyloxy derivative **33** was reacted with chloroacetylchloride in the presence of triethylamine to give **34** in 84% yield. The alkylation of **34** with **28,** followed by deprotection with tetramethylammonium hydroxide in acetone, and subsequent esterification with the alkanoylchloride gave the products **6a** and **6b**. The overall yield of **6a** from diethanolamine was 46%.

Differential scanning calorimetry showed that **6a** and **6b** alone exhibit a main phase transition at 18.8 and 37.9°C, respectively. These temperatures were quite comparable to the transition temperatures of DMPC and DPPC, (24.3 and 41°C, respectively). Liposomes prepared from boron lipids, DSPC, and cholesterol (1:1:1 mole ratio) were successfully prepared by thin film hydration and extrusion. The mean diameters of the liposomes containing **6a** and **6b** in combination with DSPC and cholesterol were found to be 135 and 123 nm, respectively. The liposomes had ξ-potentials of −67 and −63 mV, respectively, reflecting the double negative charge of the head group. Liposomes prepared from **6a** were slightly less toxic to V79 Chinese hamster cells (IC_{50} = 5.6 mM) than

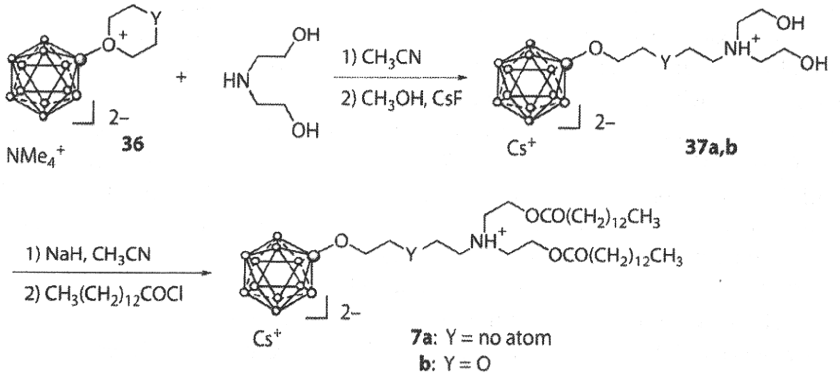

SCHEME 8.7 Synthesis of *closo*-dodecaborate lipids **7**.

unformulated BSH (IC_{50} = 3.9 mM), while liposomes prepared from **6b** were not toxic even at 30 mM (Justus et al., 2007).

Schaffran and coworkers synthesized new boron-containing lipids, which consist of a diethanolamine frame with two myristoyl chains bonded as esters (Schaffran et al., 2009b). Butylene or ethyleneoxyethylene units provide a link between the doubly negatively charged dodecaborate cluster and the amino function of the frame, obtained by nucleophilic attack of diethanolamine on the tetrahydrofuran and dioxane derivatives, respectively, of *closo*-dodecaborate (Scheme 8.7). The thermotropic behavior was found to be different for the two lipids, with the butylene lipid **7a** showing sharp melting transitions at surprisingly high temperatures. Toxicity *in vitro* and *in vivo* varied greatly, with the butylene derivative **7a** being more toxic than the ethyleneoxyethylene derivative **7b**.

Furthermore, Schaffran and coworkers developed pyridinium lipids with the dodecaborate cluster. The lipids consist of a pyridinium core with C12, C14, and C16 chains as lipid backbone, connected through the nitrogen atom through a butylene, pentylene, or ethyleneoxyethylene linker to the oxygen atom on the dodecaborate cluster as headgroup (Schaffran et al., 2009a). Synthesis of pyridinium lipids with the dodecaborate cluster is shown in Scheme 8.8. The lipids were obtained by nucleophilic attack of 4-(bisalkylmethyl)pyridine on the tetrahydrofurane **36**, the dioxane **37**, and a newly prepared tetrahydropyrane derivative **38**, respectively, of *closo*-dodecaborate. All of these boron lipids form closed vesicles in addition to some bilayers in the pure state and in the presence of helper lipids. The thermotropic behavior was found to be increasingly complex and polymorphic with increasing alkyl chain length. Except for two lipids (**9a** and **9b**), all lipids showed low *in vitro* toxicity, and longer alkyl chains led to a significant decrease in toxicity. The choice of the

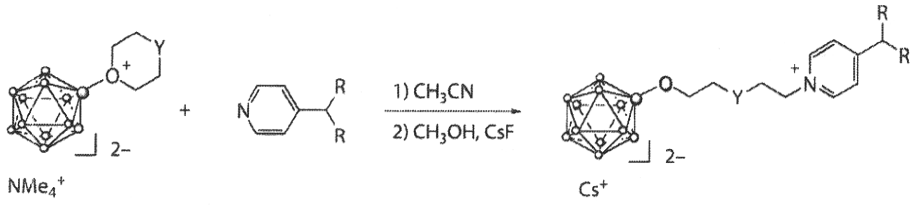

SCHEME 8.8 Synthesis of tetrahydropyran derivatives **8–10** of the *closo*-dodecaborate cluster.

linker played no major role with respect to their ability to form liposomes and their thermotropic properties, but the toxicity was influenced by the linkers in the case of short alkyl chains.

El-Zaria and Nakamura developed a new method that utilizes the click cycloaddition reaction to functionalize BSH with organic molecules (El-Zaria et al., 2009; El-Zaria et al., 2010). *S,S*-bis(propynyl)sulfonioundecahydro-*closo*-dodecaborate (1-) tetramethylammonium salt (*S,S*-dipropargyl-$SB_{12}H_{11}^-$: **41**) was prepared from BSH with propargyl bromide. Compound **41** acts as a powerful building block for the synthesis of a broad spectrum of 1,4-disubstituted 1,2,3-triazole products in high yields based on the click cycloaddition reaction mediated by Cu(II) ascorbate. The reactions require only benign reaction conditions and simple workup and purification procedures; an unsymmetric bis-triazole BSH derivative could also be synthesized by the stepwise click reaction. Synthesis of the *closo*-dodecaborate lipid with four-tailed moieties was achieved by the click cycloaddition reaction of **41** with 3-*O*-azidoacetyl-1,2-*O*-distearoyl-*sn*-3-glycerol **40**, which was readily prepared from the corresponding alcohol **26c** in two steps as shown in Scheme 8.9.

8.4 BORON CHOLESTEROL–LIPOSOME APPROACH

Cholesterol is indispensable for the formation of stable liposomes, especially in blood circulation. Therefore, the development of boronated cholesterol derivatives is considered to be an alternative approach to boron embedment in the liposome bilayer. The first boronated cholesterol derivatives were reported by Feakes et al. (1999) They introduced a *nido*-carborane into the cholesterol framework through ether or ester bonds. Although they synthesized *nido*-carborane conjugated cholesterols **42a–b** (Figure 8.6), the evaluation of their liposomes has not been reported yet.

Tjarks and coworkers developed ortho-carboranyl phenol **43** as a cholesterol mimic, which was utilized as a lipid bilayer component for the construction of nontargeted and receptor-targeted boronated liposomes. The major structural feature of the boronated cholesterol mimic is the physicochemical similarity between cholesterol and carborane frameworks (Endo et al., 1999). Cholesterol analog **43** was stably incorporated into non-, FR-, and vascular endothelial growth factor receptor-2 (VEGFR-2)-targeted liposomes. No major differences in appearance, size distribution, and lamellarity were found among conventional DPPC/cholesterol liposomes, nontargeted, and FR-targeted liposomal formulations of this carboranyl cholesterol derivative. FR-targeted boronated liposomes were taken up extensively by FR-overexpressing KB cells *in vitro*, and the uptake was effectively blocked in the presence of free folate. There was no apparent *in vitro* cytotoxicity in FR-overexpressing KB cells and VEGFR-2-overexpressing 293/KDR cells when these were incubated with boronated FR- and (VEGFR-2)-targeted liposomes, respectively, although the former accumulated extensively in KB cells and the latter effectively interacted with VEGFR-2 by causing autophosphorylation and protecting 293/KDR cells from SLT (Shiga-like toxin)-VEGF cytotoxicity (Thirumamagal et al., 2006).

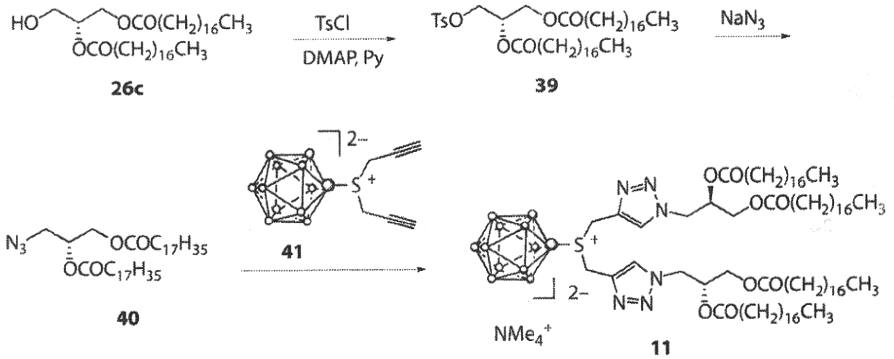

SCHEME 8.9 Synthesis of the *closo*-dodecaborate lipid **11** by the click cycloaddition reaction.

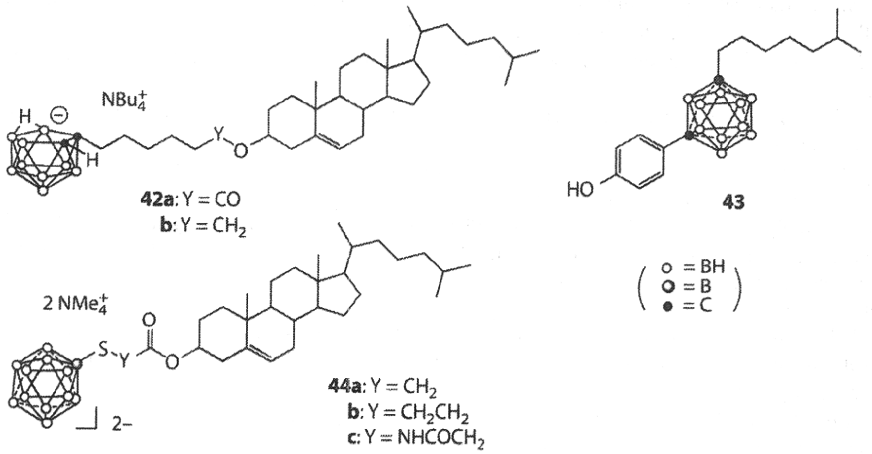

FIGURE 8.6 Structures of cholesterol-boron cluster conjugates (**42** and **44**) and ortho-carboranyl phenol **43**.

Nakamura, Gabel, and coworkers developed *closo*-dodecaborate conjugated cholesterols **44a–c**. The closo-dodecaborate conjugated cholesterol **44a** liposome, which was prepared from dimyristoylphosphatidylcholine, cholesterol, **44a**, and PEG-conjugated distearoylphosphatidylethanolamine (1:0.5:0.5:0.1), exhibited higher cytotoxicity than BSH at the same boron concentration and the IC_{50} values of **44a** liposome and BSH toward colon 26 cells were estimated to be 25 and 78 ppm of boron concentration, respectively (Nakamura et al., 2007b).

8.5 SUMMARY

Recent development of liposomal BDS are summarized in this chapter. Two approaches to encapsulation of boron compounds into liposomes and incorporation of boron-conjugated lipids into the liposomal bilayer have been investigated. Since the leakage upon storage has been observed in boron-encapsulated liposomes, the combination of both approaches would be more potent to carry a large amount of ^{10}B compounds into tumor. In general drug delivery systems, liposomes are used for selective delivery of drugs to tumors in an effort to avoid the drugs from undesirably accumulating in other organs. However, a large amount of liposomes that are administrated accumulate in the liver and may cause severe side effects for patients. BDS, in this context, is a safer system because boron compounds delivered with liposomes are nontoxic unless neutron capture reaction of boron takes place. Therefore, the boron compounds accumulated in other organs will not cause side effects for the patient under condition that the boron compounds are nontoxic. Liposomal drug delivery system is variable depending on tumoral blood vessel formations and diffusion processes for the liposomes to reach deeper portion in tumors, thus it is important to choose the target cancers that are considered to be suitable for treatment with BDS. In this regards, liposomal BDS targeted to brain tumor is not a suitable strategy although brain tumors still are the major target for BNCT. Since successful BNCT is highly dependent on the selective and significant accumulation of boron-10 in tumor cells, liposomal BDS would be one of the efficient approaches for the treatment of a variety of cancers with BNCT.

REFERENCES

Aihara, T., Hiratsuka, J., Morita, N. et al. 2006. First clinical case of boron neutron capture therapy for head and neck malignancies using 18f-bpa pet. *Head Neck* 28: 850–5.

Allen, T. M. 1998. Liposomal drug formulations: Rationale for development and what we can expect for the future. *Drugs* 56: 747–56.

Bangham, A. D., Standish, M. M., and Watkins, J. C. 1965. Diffusion of univalent ions across the lamellae of swollen phospholipids. *J. Mol. Biol.* 13: 238–52, IN26–7.

Barth, R. 2003. A critical assessment of boron neutron capture therapy: An overview. *J. Neuro-Oncol.* 62: 1–5.

Barth, R. F. 2009. Boron neutron capture therapy at the crossroads: Challenges and opportunities. *Appl. Radiat. Isot.* 67: S3–6.

Barth, R. F., Coderre, J. A., Vicente, M. G. et al. 2005. Boron neutron capture therapy of cancer: Current status and future prospects. *Clin. Canc. Res.* 11: 3987–4002.

Betageri, G. V., Jenkins, S. A., and Parsons, D. L. 1993. *Liposome Drug Delivery Systems*. Basel: Technomic.

El-Zaria, M. E., Genady, A. R., and Nakamura, H. 2010. Synthesis of triazolyl methyl-substituted amino- and oxy-undecahydrododecaborates for potential application in boron neutron capture therapy. *New J. Chem.*: Q9 In press.

El-Zaria, M. E. and Nakamura, H. 2009. New strategy for synthesis of mercaptoundecahydrododecaborate derivatives via click chemistry: Possible boron carriers and visualization in cells for neutron capture therapy. *Inorg. Chem.* 48: 11896–902.

Endo, Y., Iijima, T., Yamakoshi, Y. et al. 1999. Potent estrogenic agonists bearing dicarba-closo-dodecaborane as a hydrophobic pharmacophore. *J. Med. Chem.* 42: 1501–04.

Feakes, D. A., Shelly, K., and Hawthorne, M. F. 1995. Selective boron delivery to murine tumors by lipophilic species incorporated in the membranes of unilamellar liposomes. *Proc. Natl. Acad. Sci.* 92: 1367–70.

Feakes, D. A., Shelly, K., Knobler, C. B. et al. 1994. Na3[b20h17nh3]: Synthesis and liposomal delivery to murine tumors. *Proc. Natl. Acad. Sci.* 91: 3029–33.

Feakes, D. A., Spinler, J. K., and Harris, F. R. 1999. Synthesis of boron-containing cholesterol derivatives for incorporation into unilamellar liposomes and evaluation as potential agents for BNCT. *Tetrahedron* 55: 11177–86.

Gabel, D., Moller, D., Harfst, S. et al. 1993. Synthesis of *s*-alkyl and *s*-acyl derivatives of mercaptoundecahydrododecaborate, a possible boron carrier for neutron capture therapy. *Inorg. Chem.* 32: 2276–78.

Haritz, D., Gabel, D., and Huiskamp, R. 1994. Clinical phase-i study of na2b12h11sh (bsh) in patients with malignant glioma as precondition for boron neutron capture therapy (BNCT). *Int. J. Radiation Oncology Biol. Phys.* 28: 1175–81.

Hawthorne, M. F. 1993. The role of chemistry in the development of boron neutron capture therapy of cancer. *Angew. Chem. Int. Ed. Engl.* 32: 950–84.

Ishida, O., Maruyama, K., Tanahashi, H. et al. 2001. Liposomes bearing polyethyleneglycol-coupled transferrin with intracellular targeting property to the solid tumors *in vivo*. *Pharm. Res.* 18: 1042–8.

Justus, E., Awad, D., Hohnholt, M. et al. 2007. Synthesis, liposomal preparation, and *in vitro* toxicity of two novel dodecaborate cluster lipids for boron neutron capture therapy. *Bioconjugate Chem.* 18: 1287–93.

Kato, I., Ono, K., Sakurai, Y. et al. 2004. Effectiveness of bnct for recurrent head and neck malignancies. *Appl. Radiat. Isot.* 61: 1069–73.

Kullberg, E. B., Carlsson, J., Edwards, K. et al. 2003. Introductory experiments on ligand liposomes as delivery agents for boron neutron capture therapy. *Int. J. Oncol.* 23: 461–7.

Kunitake, T. 1992. Synthetic bilayer membranes: Molecular design, self-organization, and application. *Angew. Chem. Int. Ed. Engl.* 31: 709–26.

Kunitake, T. and Okahata, Y. 1977. A totally synthetic bilayer membrane. *J. Am. Chem. Soc.* 99: 3860–61.

Lee, J.-D., Ueno, M., Miyajima, Y. et al. 2007. Synthesis of boron cluster lipids: Closo-dodecaborate as an alternative hydrophilic function of boronated liposomes for neutron capture therapy. *Org. Lett.* 9: 323–26.

Li, T., Hamdi, J. and Hawthorne, M. F. 2006. Unilamellar liposomes with enhanced boron content. *Bioconjugate Chem.* 17: 15–20.

Maeda, H., Wu, J., Sawa, T. et al. 2000. Tumor vascular permeability and the EPR effect in macromolecular therapeutics: A review. *J. Controlled Release* 65: 271–84.

Maruyama, K. 2000. *In vivo* targeting by liposomes. *Biol. Pharm. Bull.* 23: 791–99.

Matsumura, Y. and Maeda, H. 1986. A new concept for macromolecular therapeutics in cancer chemotherapy: Mechanism of tumoritropic accumulation of proteins and the antitumor agent SMANCS. *Cancer Res.* 46: 6387–92.

Menger, F. M. and Gabrielson, K. D. 1995. Cytomimetic organic chemistry: Early developments. *Angew. Chem. Int. Ed. Engl.* 34: 2091–106.

Mishima, Y., Ichihashi, M., Hatta, S. et al. 1989. New thermal neutron capture therapy for malignant melanoma: Melanogenesis-seeking 10b molecule-melanoma cell interaction from *in vitro* to first clinical trial. *Pigment Cell Res.* 2: 226–34.

Expert Opinion

Hypoxia-inducible factor inhibitors: a survey of recent patented compounds (2004 – 2010)

Hyun Seung Ban, Yoshikazu Uto & Hiroyuki Nakamura†
†*Gakushuin University, Department of Chemistry, Faculty of Science, 1-5-1, Mejiro, Toshima-ku, Tokyo, 171-8588, Japan*

Introduction: Hypoxia-inducible factor (HIF) is a heterodimeric transcription factor consisting of α and β subunits that regulates the expression of angiogenic factors, including VEGF, which are involved in angiogenesis, invasion/metastasis, glucose uptake and cell survival during cancer development.
Areas covered: This review summarizes the information about patented HIF inhibitors over the last 7 years (2004 – 2010). The reader will gain an outline of the structure and biological activity of recently developed HIF inhibitors.
Expert opinion: Inhibition of HIF is an attractive therapeutic target for tumor angiogenesis and, until now, various HIF inhibitors have been discovered and evaluated. It is expected that development of more potent and selective HIF inhibitors will provide an effective treatment of cancer and other HIF-related diseases, including inflammation and cardiovascular disorder. As VEGF plays an important role in angiogenesis during tumor growth and ischemic diseases, the inhibition of VEGF-induced HIF is an attractive approach for the suppression of hypoxia-mediated pathological angiogenesis. HIF inhibitors may not only have cytostatic antitumor effects with fewer side effects, but also synergetic effects combined with radiotherapy.

Keywords: angiogenesis, cancer, HIF, HIF inhibitors, hypoxia

Expert Opin. Ther. Patents [Early Online]

1. Introduction

Hypoxia-inducible factor (HIF), a member of Per-aryl hydrocarbon receptor nuclear translocator (ARNT)-Sim family of heterodimeric basic helix-loop-helix transcription factor, consists of α subunits (HIF-1α, -2α and -3α) and β subunit (HIF-1β, which is also known as ARNT) [1-3]. Under aerobic condition, post-translational hydroxylation of proline residues (Pro402 and Pro564) in the oxygen-dependent degradation domain of HIF-1α is induced by oxygen-sensitive dioxygenases catalyzing prolyl hydroxylase (PHD). The hydroxylated HIF-1α binds to the von Hippel-Lindau (VHL) tumor suppressor protein, a component of the E3 ubiquitin ligase complex [4-7]. These interactions lead to the rapid degradation of HIF-1α through an ubiquitin and proteasome-dependent pathway [8-10]. Beside proline hydroxylation, asparagine (Asn803) in the C-terminal transactivation domain (CAD) of HIF-1α is hydroxylated by the factor-inhibiting HIF (FIH), an oxygen-dependent hydroxylase enzyme under aerobic condition [11]. This modification inhibits HIF transcriptional activity by preventing the interaction between CAD and p300/CBP transcriptional co-activator. Under hypoxic condition, HIF-1α is stabilized due to hypoxia-mediated reduction of PHD and FIH activities and is translocated into the nucleus, where it dimerizes with the constitutively expressed HIF-1β [12,13]. The HIF-1α and -β heterodimers bind to a *cis*-acting regulatory element referred to as

informa
healthcare

10.1517/13543776.2011.547477 © 2011 Informa UK, Ltd. ISSN 1354-3776

Article highlights.

- The hypoxia-inducible factor (HIF) is a heterodimeric transcription factor consisting of α and β subunits that take part in the expression of hypoxia-responsive genes involved in angiogenesis, invasion/metastasis, glucose uptake and cell survival during cancer development.
- As VEGF plays an important role in angiogenesis during tumor growth and ischemic diseases, the inhibition of VEGF-induced HIF is an attractive approach for the suppression of hypoxia-mediated pathological angiogenesis.
- HIF-1 inhibitors interfere with HIF-1α synthesis, folding, stabilization and nuclear transduction.
- The most important HIF-1α regulatory systems are PI3K/Akt/mTOR, MAPK, the HSP90 system, topoisomerase I and Trx-1, and clinical trials have been carried out with several HIF-1 inhibitors, including tenaspimycin, PX-866, PX-12, EZN-2968 and PX-478.

This box summarizes key points contained in the article.

hypoxia-response element (HRE) (5′-RCGTG-3′, where R is A or G) in the promoter region of a number of genes, including glucose transporters, glycolytic enzymes, angiogenic growth factors, and several molecules involved in apoptosis and cell proliferation such as erythropoietin (EPO), transferrin, endothelin-1, iNOS, heme oxygenase 1, VEGF, IGF and IGF-binding proteins [14,15].

Until now, physiological and pathological implications of HIF in various human diseases including inflammation, cardiovascular disorder and cancer have been clarified [16-18]. Especially during cancer development, HIF-1α is a key regulator of the expression of various genes associated with tumor angiogenesis, metastasis, invasion, proliferation and apoptosis. Overexpression of HIF-1α has been observed in human cancers including brain, breast, colon, lung, ovary and prostate cancers [19], and HIF-1α is implicated in treatment resistance and poor prognosis in the hypoxic region around cancer. Therefore, drugs targeting HIF-1α have the potential to target multiple cancer processes, and a large number of HIF inhibitors have been developed. Several HIF inhibitors have entered clinical trials. This survey reviews the patent literature of HIF inhibitors and clinical trials reported in the last 7 years (**Figure 1**).

2. Small molecule HIF inhibitors

2.1 PX-12

Thioredoxin-1 (Trx-1) is a cellular redox protein that promotes tumor growth, inhibits apoptosis and upregulates HIF-1α and VEGF. PX-12 (1-methylpropyl 2-imidazolyl disulfide, compound 1 in **Figure 2**) has shown both excellent *in vitro* and promising *in vivo* antitumor activity, irreversibly thio-alkylating the Cys73 thioredoxin residue [20]. PX-12 inhibition of Trx-1 results in subsequent inhibition of the hypoxia-induced increase in HIF-1α protein and VEGF secretion [21]. PX-12 is rapidly metabolized, providing two inactive metabolites, volatile 2-butanethiol and 2-mercaptoimidazole (**Figure 2**).

PX-12 was tested in Phase I pharmacokinetic and pharmacodynamic study in patients with advanced solid tumors. Thirty-eight patients with advanced solid tumors received PX-12 at doses of 9 – 300 mg/m^2, as 1- or 3 h intravenous infusion on days 1 – 5, repeated every 3 weeks. The best response was stable disease (SD) in seven patients (126 – 332 days). PX-12 treatment lowered plasma Trx-1 concentrations in a dose-dependent manner. PX-12 was tolerated up to a dose of 226 mg/m^2 by a 3 h infusion [22,23]. However, a randomized Phase II study of PX-12 in patients with advanced cancer of the pancreas following progression after a gemcitabine-containing combination resulted in the lack of significant antitumor activity and unexpectedly low baseline Trx-1 levels. PX-12 does not appear to be active in unselected patients with previously treated advanced pancreatic cancer. Thus, the study was terminated [24].

2.2 PX-478

PX-478 (*S*-2-amino-3-[4′-*N*,*N*,-bis(2-chloroethyl)amino]phenyl propionic acid *N*-oxide dihydrochloride, compound 2 in **Figure 2**) suppresses constitutive and hypoxia-induced levels of HIF-1α protein in various cancer cells in a pVHL and p53-independent manner [25].

A patent application from ProlX Pharmaceuticals claimed that *N*-oxides of melphalan derivatives are HIF-1α inhibitors useful for the treatment of diseases associated with HIF, including choroidal and retinal neovascularization, age-related macular degeneration, joint disease, inflammation, neurodegenerative diseases and ischemic neperfusion injury [26]. Various biological data were provided in this patent application. PX-478 inhibited the hypoxia-induced expression of HIF-1α in prostate cancer PC-3, breast cancer MCF-7 and colon cancer HT-29 cells without affecting the HIF-1β level, and IC_{50} values were 2.1, 3.5 and 17.8 μM, respectively. PX-478 also inhibited the hypoxia-induced HIF transactivation in MCF-7 and HT-29 cells with IC_{50} values of 20.5 and 23.1 μM, respectively. Furthermore, IC_{50} values for inhibition of the hypoxia-induced VEGF secretion into the medium was 3.8 and 11.5 μM in MCF-7 and HT-29 cells, respectively. The detailed mechanism of action of HIF-1α inhibition by PX-478 was claimed in another patent application from ProlX Pharmaceuticals [27]. PX-478 inhibited HIF-1α expressions in RCC4 (human renal carcinoma cells lacking the VHL gene), indicating that PX-478 suppresses HIF-1α via a VHL-independent pathway. It has been reported that tumor suppressor p53 binds to HIF-1α allowing recruitment of MDM2, an E3 ubiquitin-ligase, resulting in the degradation of both p53 and HIF-1α [28]. PX-478 suppressed the HIF-1α expression in human colon cancer HCT116$^{-/-}$ cells lacking p53, demonstrating that it is not acting by a p53-dependent mechanism. The inhibition of HIF-1α

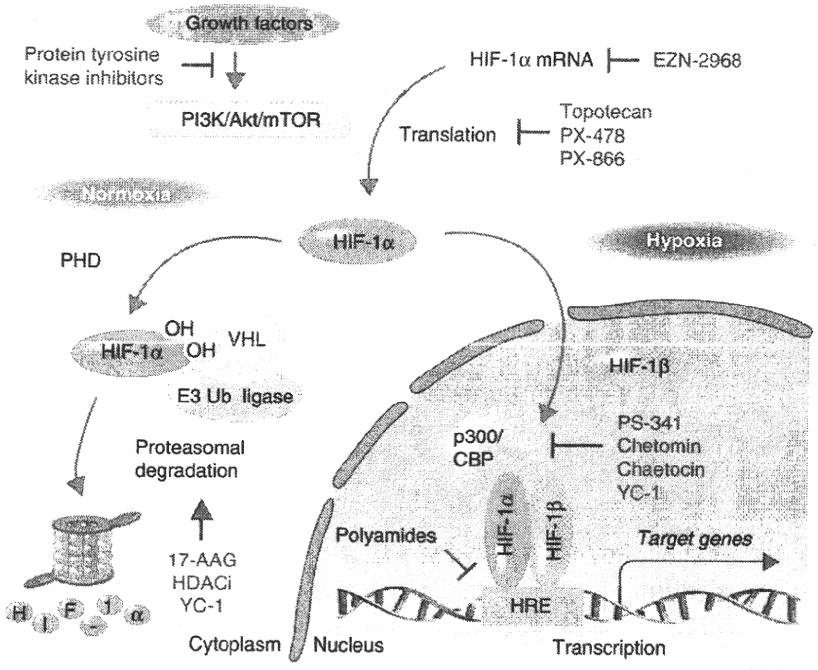

Figure 1. HIF signaling and inhibitors.

expression by PX-478 was proteasome-dependent degradation, and PX-478 increased the level of ubiquitinated HIF-1α through the prevention of deubiquitination of HIF-1α. *In vivo* MCF-7 or HT-29 xenograft model showed that treatment with PX-478 significantly decreased tumor growth and the expression of HIF-1α [26,27,29]. Recently, the Board of Regents of the University of Texas System reported the pharmaceutical compositions of PX-478 for the treatment of small cell lung cancers (SCLC) and the methods of inhibiting metastasis and the combination with radiation, photodynamic therapy and anti-angiogenic agents [30]. PX-478 was effective at both the high (20 mg/kg) and low (10 mg/kg) doses in reducing the tumor volume and weight against the SCLC orthotopic model.

PX-478 was tested in a Phase I, dose escalation study in patients with advanced solid tumors. Forty patients received doses between 1 and 88.2 mg/m^2 orally on days 1 – 5 of a 21 day cycle. Best response was SD in 14/36 evaluable patients. Patients with SD received a median of 4 cycles (range 2 – 16); four patients received ≥ 6 cycles (adenoid cystic, pheochromocytoma, prostate and vaginal cancers). PX-478 has been well tolerated and associated with prolonged SD in patients with advanced cancers. Inhibition of HIF-1α despite low PX-478 levels is consistent with the idea that active metabolites other than melphalan may be responsible for the pharmacodynamic observations. These data support the continued evaluation of HIF-1α inhibition as a therapeutic target [31].

2.3 YC-1 derivatives

YC-1 (3-(5′-hydroxymethyl-2′-furyl)-1-benzylindazole, compound 3 in **Figure 2**) is a soluble guanylyl cyclase (sGC) activator that is primarily developed for the treatment of circulation disorders through inhibition of platelet aggregation and vascular contraction [32,33]. In 2001, Yeo and co-workers found that YC-1 completely blocks the HIF-1α expression at the post-transcriptional level and consequently inhibits the transcription factor activity of HIF under hypoxic condition. In addition, sGC inhibitors did not block the inhibitory effects of YC-1 on HIF, and 8-bromo-cGMP did not inhibit the hypoxia-induced expression of HIF [34]. These results indicate that the inhibition of HIF by YC-1 is sGC-independent action. Thus, YC-1 is recognized as an HIF inhibitor and antitumor agent.

A patent application from HIF Bio, Inc. claimed the use of YC-1 and its derivatives for the inhibition of HIF-1α expression in tumors, including hepatoma, stomach carcinoma, renal carcinoma, cervical carcinoma and neuroblastoma [35]. YC-1 inhibited the hypoxia-induced expression of HIF-1α and its target genes include VEGF, aldolase A and enolase 1 in various cancer cells such as Hep3 G hepatoma, NCI-H87 gastric carcinoma, SiHa cervical, SK-N-MC neuroblastoma and Caki-1 renal carcinoma cells. Almost complete inhibition was observed at the concentration of 10 μM. In the *in vivo* tumor xenograft model, treatment with 30 mg/kg of YC-1 suppressed the growth of tumor cells. In this model, immunohistochemical analysis with tumor

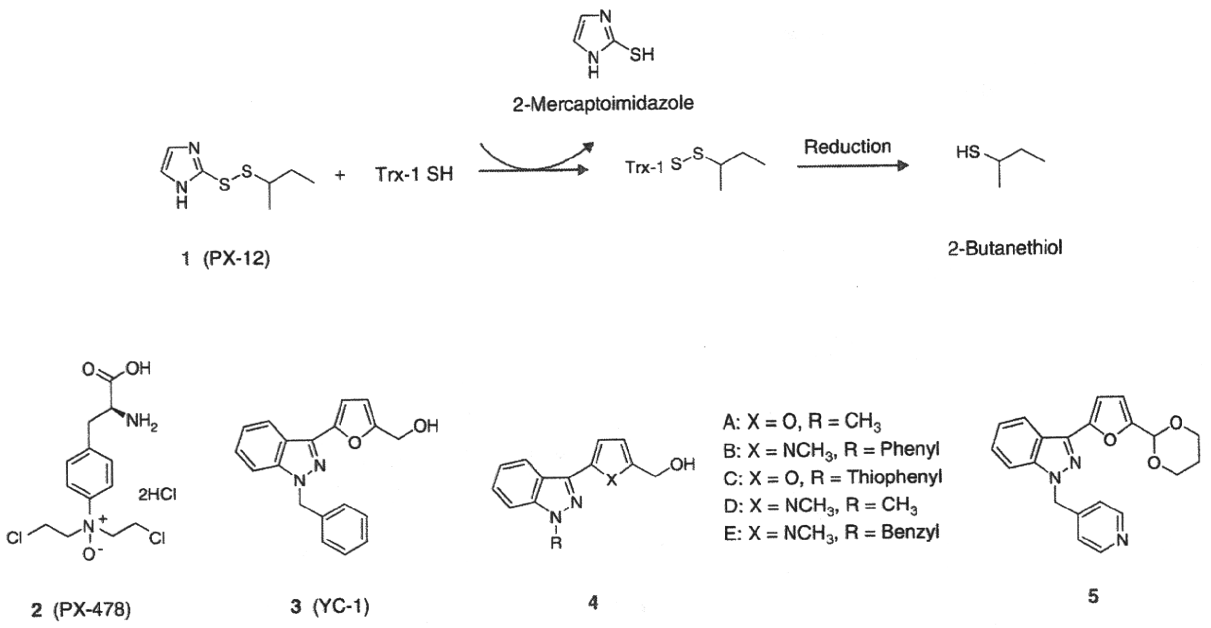

Figure 2. PX-12, PX-478 and YC-1 derivatives.

sections showed that YC-1 reduced the amount of HIF-1α-positive cells and endothelial marker CD31-positive cells. These results indicate that the tumor growth inhibition by YC-1 is mediated by suppression of HIF-1α expression. This application also claimed the use of YC-1 and its derivatives in combination with other anticancer agents. HIF Bio further claimed a series of YC-1 derivatives (compounds **4A–D** in **Figure 2**) [36]. Under hypoxic condition, compounds **4A–D** suppressed the hypoxia-induced expression of HIF-1α similar to YC-1 at the concentration range of 0.3 – 10 μM. The ability of the compounds to inhibit tumor growth was determined in male nude mice following subcutaneous injection of Hep3B hepatoma cells. After the xenografted tumors reached 100 – 150 mm^3 in size, compounds were treated by intraperitoneal injection daily for 2 weeks. At the end of the treatment period, compounds reduced the tumor size from about 900 mm^3 in vehicle-treated controls to about 400 mm^3 at doses of 10 mg/kg/day (compounds **4A–D**) or 30 mg/kg/day (compounds **4A** and **B**). Another patent application from HIF Bio claimed to have a series of heterocycle-substituted pyrazoles, such as compound **5** (**Figure 2**), for the treatment of HIF-related and VEGF-mediated disease or disorder [37]. However, no biological data were presented.

2.4 Benzopyran derivatives

A series of 2,2-dimethyl-2*H*-chromene (2,2,-dimethylbenzopyran) derivatives has been developed as inhibitors of the HIF-1 pathway. The first examples of benzopyran-based HIF-1 inhibitors were patented by researchers from Emory University and Scripps Research Institute in 2004 [38]. These novel benzopyrans were tested for their inhibitory activity on the HIF-1–HRE pathway using LN229 glioma cells expressing the alkaline phosphatase reporter gene. The most potent compound **6** (**Figure 3**) displayed an IC_{50} value of 7.5 μM. Following this first patent, the same group reported an additional series of 2,2-dimethylbenzopyran derivatives in 2007 [39]. A library of 2,2-dimethylbenzopyran derivatives (> 10,000) were prepared by combinatorial synthesis [40-42]. Screening of the library in the cell-based HIF-1–HRE assay resulted in the discovery of highly potent HIF-1 inhibitors, such as KCN-1 (compound **7** in **Figure 3**) with an IC_{50} value of ~ 4 μM. Further analysis showed that KCN-1 reduced hypoxic levels of HIF-1α in glioma cell lines without significantly affecting the levels of HIF-1β. For *in vivo* pharmacological evaluation, KCN-1 was evaluated in nude mice with sc LN229 glioma xenograft implants. A strong and sustained inhibition of tumor growth was observed without any significant weight changes or behavioral abnormalities after intraperitoneal administration of KCN-1 at a dose of 60 mg/kg for 5 days. Further structural optimization provided detailed SAR information. In short: i) dimethoxy substitution on the left-hand phenyl is preferred, ii) amide or aliphatic bond is also permitted in place of sulfonamide, iii) flexible rings are favored over *N*-aromatic rings and flexible aliphatic chains are preferred and iv) addition of hydrophilic groups is tolerated on benzopyran. More recently, structurally related 2,2-benzopyran derivatives (compounds **8** and **9** in **Figure 3**) were also shown to inhibit the HIF-1–HRE pathway [43,44].

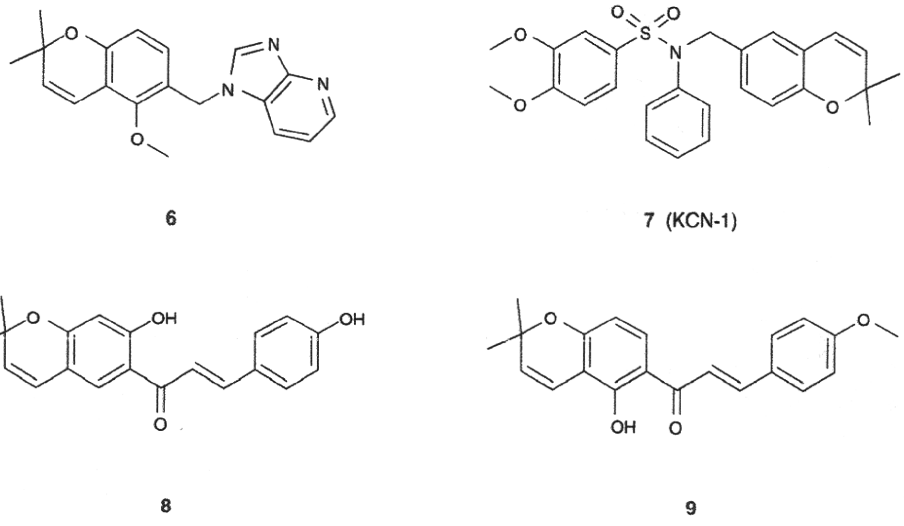

Figure 3. Benzopyran derivatives.

2.5 Aromatic compounds and heteroaryls

Due to the complexity of the biological processes that regulate the HIF-1 pathway, a wide variety of structural motifs have been reported to inhibit HIF-1 activity. For example, a group from the National Cancer Institute evaluated numerous tricyclic compounds using HIF-1 reporter luciferase assay in recombinant U251 human glioma cells [45]. One of the examples (NSC 644221, compound **10** in **Figure 4**) originally reported as a weak DNA-binding intercalating agent [46] was further evaluated and shown to decrease hypoxic induction of luciferase expression in a dose-dependent fashion (EC_{50} ~ 1 μM) in the U251-HRE cell assay [47]. The specificity on HRE was clearly indicated by the fact that NSC 644221 did not significantly affect the constitutive luciferase expression in the control cell line U251-pGL3 up to 10 μM. Interestingly, it was shown that NSC 644221 did not inhibit the HIF-1α expression when cells were transfected with siRNA targeting topoIIa.

Novel thiazolidinone compounds were claimed by Cell Therapeutics Europe S.R.L. to inhibit HIF-1α–p300 interaction and prevent VEGF production in tumor cells under hypoxia conditions. One of the examples (compound 11 in **Figure 4**) demonstrated its ability to disrupt HIF-1α–p300 interaction with an IC_{50} value of 1.4 μM in a fluorescence assay (DELIFIA™) [48].

The University of Texas reported that imidazo[1,2-a] pyrazine-based tyrosine kinase inhibitors, exemplified by compound 12 (**Figure 4**), inhibited HIF-1 expression and HIF-signal transduction pathways [49]. Influence of these tyrosine kinase inhibitors on HIF was tested on C6#4 cells. Compound 12 showed EC_{50} values of 2.2 and 19.6 μM with respect to G/R (GFP/RFP expression, HIF-1α inhibitory activity) and WST-1 (cell viability).

In a patent application filed by Piramal [50], small molecule compounds that contain the 2-chloro-*N*-pyridin-3-ylacetamide moiety were tested in U251 human glioma cells stably transfected with human HRE and the U251 pGL3 cells (control cell line). Specificity index (SI) and the ratio of IC_{50} under normoxic condition to hypoxia condition were measured for selected compounds in the patent. One of the examples (compound **13A** in **Figure 4**) exhibited SI > 20 in the assay. Recently, a related analog was reported as P2630 (compound **13B**) [51]. P2630 exhibited strong HIF-1α inhibitory activity under hypoxic (1% O_2) conditions with an IC_{50} value of 0.8 μM and marginal inhibitory activity under normoxic (21% O_2) conditions. Anti-proliferative activity was tested in ^{3}H-thymidine incorporation assay across different cancer cell lines (PC-3, DU-145, U251, HCT-116, Ovcar-3 and Panc-1) and normal cell lines (MRC-5 and WI-38). P2630 showed best anti-proliferative activity in the PC-3 cell line (IC_{50}: 1.0 μM), while it did not potently inhibit the proliferation of normal cell lines (IC_{50}: > 10 μM for MRC-5; 6.5 μM for WI-38). *In vivo* efficacy was evaluated in the SCID mice with PC-3 xenograft. After a 19-day oral administration (50 mg/kg twice daily), P2630 demonstrated significant tumor growth inhibition without substantial weight loss.

Thalidomide analogs were previously reported to possess anti-angiogenic activity in a HUVEC assay [52]. In 2008, Charlesson LLC claimed that the thalidomide analogs were suppressors of HIF-1α expression and useful for the treatment of vascular abnormalities such as neovascularization and vascular leakage [53]. The thalidomide analogs in this patent significantly suppressed the HIF-1α expression in PC-3 prostate cancer cells by ~ 79 – 90% at the tested concentration (10 μM). According to the data demonstrated in this patent, the thalidomide analogs have promising effects for the

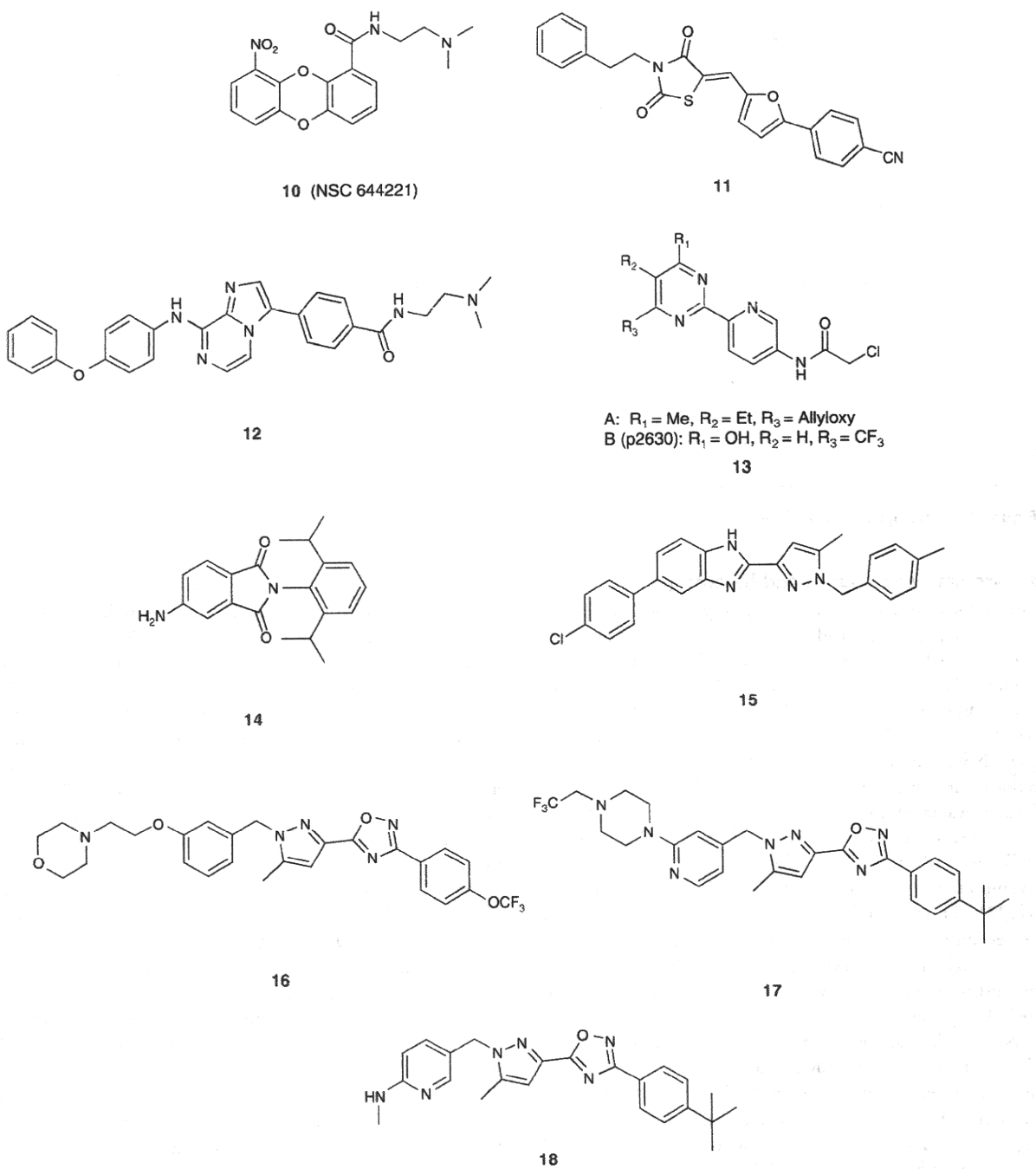

Figure 4. Aromatic compounds and heteroaryls.

treatment of ocular disease, particularly diabetic retinopathy. CLT-003 (compound 14 in Figure 4) was intravitreally injected (5 µl/eye, 0.8 mM in BN rat serum) to the right eye and the same volume of vehicle was injected to the left eye of streptozotocin-treated diabetic rats. Measurement of retinal vascular permeability by Evans blue-albumin method after 2 days of injection showed that CLT-003 significantly reduced retinal vascular leakage by 100% (n = 6). CLT-003 has been developed as a clinical candidate by Charlesson LLC to primarily target diabetic macular edema.

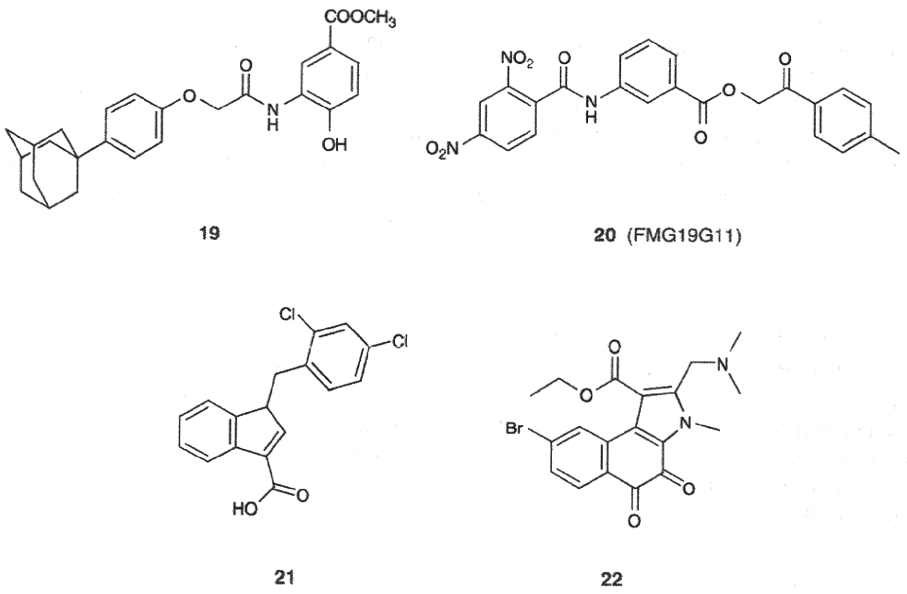

Figure 4. Aromatic compounds and heteroaryls (continued).

For secondary indications, macular edema secondary to other pathologies and wet age-related macular degeneration are also suggested [54].

Bayer Schering Pharma disclosed a patent application describing novel heteroaryl-substituted pyrazole compounds as modulators of HIF-1α for the treatment of hyperproliferative disorders and diseases associated with angiogenesis [55]. These pyrazole derivatives were tested in HIF-luciferase assay using HCT-116 cells. One of the examples (compound **15** in **Figure 4**) exhibited an IC_{50} value of 0.003 μM in the assay. Recently, they disclosed an additional series of novel pyrazole derivatives, especially 5-(5-methyl-1*H*-pyrazol-3-yl)-1,2,4-oxadiazole analogs (compounds **16** – **18** in **Figure 4**) as highly potent HIF inhibitors [56-58]. Some of these pyrazole derivatives showed very strong inhibition toward HIF-1 transcriptional activity in the luciferase assay with IC_{50} values in the range of sub-nanomolar.

Korea Research Institute of Bioscience and Biotechnology claimed novel aryl and heterocyclic derivatives as HIF inhibitors for the treatment and prevention of cancer [59]. Compound **19** (**Figure 4**) inhibited the hypoxia-induced accumulation of HIF-1α and the expression of HIF-1 target genes EPO and VEGF without affecting HIF-1β expression in human hepatocellular carcinoma cell lines Hep3B. Administration of compound **19** at the dose of 20 or 50 kg/ml inhibited the growth of tumor in the MDA-MB-435 implanted nude mouse model. Recently, the action mechanism of compound **19** has been reported to promote proteasomal degradation of HIF-1α through upregulation of VHL [60]. Furthermore, Lee *et al.* reported inhibitory effects of (aryloxyacetylamino)benzoic acid analogs on HIF-1 transcriptional activity [61] and found that the benzimidazole analog is a novel HIF inhibitor that regulates the stability of HIF-1α through the heat-shock protein (HSP) 90-Akt pathway, leading to the degradation of HIF-1α [62]. The ortho-carborane analogs of compound **19** were reported as potent inhibitors of the hypoxia-induced activation of HIF [63]. The detailed mechanistic study using their chemical probes revealed that the target molecule of the ortho-carborane analogs was identified to be HSP60 [64].

A group from Centro de Investigacion Principe Felipe claimed that a series of benzamide derivatives could modulate and/or inhibit the transcription of genes modulated by HIF [65]. Screening of approximately 12,000 compounds using luciferase reporter gene-based assay containing 9 repetitions of the HRE 5′ upstream of the start codon in the active promoter region constitutively expressed in the HeLa cell line (HeLa-9x-HRE-Luc) resulted in the discovery of FMG19G11 (compound **20** in **Figure 4**) [66]. This compound was shown to reduce hypoxia-induced luciferase activity with an IC_{50} value of 80 nM in the HeLa-9x-HRE-Luc assay. While specific data were not shown, it was suggested that FMG19G11 inhibited transcriptional activity of HIFα not only in HeLa cell line but also in adult human cell lines from various tissues such as colon HT-29 and the breast cancer cell line MDA-MB-435-S. Notably, FM19G11 had a similar effect on HIF regulation in stem cells. Further experiments revealed that FMG19G11 demonstrated dose-dependent inhibitory activity on HIFα protein accumulation in adult rat epSPC. As for toxicity, FMG19G11 did not show any cytotoxicity on the HeLa cell line up to 30 μM in the standard oxygen tension or 50 μM under hypoxic conditions. Recent publication from

the same group reported that FMG19G11, in response to rapid hyper-activation of the growth signaling pathway through mTOR, triggered a DNA damage response associated with G(1)/S-phase arrest in a p53-dependent fashion [67].

A series of lonidamine analogs were claimed by Threshold Pharmaceuticals to be HIF-1α inhibitors [68]. The anticancer drug lonidamine (compound 21 in **Figure 4**) inhibited the hypoxia-induced HIF-1α expression in nuclear and whole cell extract of LNCaP and PC-3 cells at the concentration range of 100 – 600 μM, and a complete inhibition was observed at 400 μM.

A patent application from Cell Therapeutics Europe S.R.L. claimed that novel indole derivatives inhibit the interaction between HIF and its co-activator p300 [69]. Among the indole derivatives, compound 22 (**Figure 4**) prevented binding of HIF and p300 with an IC_{50} value of 1.5 μM, and showed the most potent inhibitory activity in VEGF-luciferase Hep3B cells with an IC_{50} value of 0.26 μM.

3. Steroidal HIF inhibitors

A patent application from Bionaut International claimed a series of steroidal compounds as HIF inhibitors [70]. Results from the screening of anti-neoplastic agents with thousands of compounds showed that cardiac glycosides, redox effectors and steroid signal modulators were highly effective agents for the treatment of neoplastic disorder, particularly HIF-positive tumor cells, pancreatic, lung, colon, prostate, cervical, renal, uterine and breast cancers. Among the cardiac glycosides including ouabain, digitoxigenin, digoxin and lanatoside C, ouabain (compound 23 in **Figure 5**), also known as strodival, potently inhibited HIF-responsive reporter activity in NSCLC A549 cell lines. Also, additive effects were observed by a combination of ouabain with redox effector niclosamide [70]. As ouabain had been identified as a Na^+/K^+ ATPase inhibitor, another patent claimed that Na^+/K^+ ATPase inhibitors such as proscillaridin (compound 24 in **Figure 5**), also known as talusfn, and marinobufagenin can be used either alone or in combination with other anticancer agents for more effective treatment of refractory cancer including pancreatic cancer [71-74]. Both proscillaridin and ouabain strongly inhibited the hypoxia-induced increase in the level of HIF-1α and production of VEGF in A549 cells. The action mechanism of HIF-1α inhibition by the cardiac glycoside compounds was described as the production of reactive oxygen species (ROS) which leads to the ubiquitylation and degradation of HIF-1α. Ouabain induced ROS in various cancer cells including A549, Caki-1 and Panc-1 cells. Also, catalase inhibited the ouabain-mediated reduction of HIF-1α protein, indicating that ouabain inhibits the HIF-1α expression through an increase in ROS production. Panc-1 implanted xenograft in a nude mouse model showed that administration of ouabain almost completely inhibited tumor growth and that additive antitumor activity was observed by co-administration with anticancer agent gemcitabine [73,74]. In 2007, Bionaut International further reported several steroidal HIF modulators including bufalin, digitoxigenin, digoxin, lanatoside C, strophantin K, uzarigenin, ouabain and proscillaridin, and their use for treatment of ocular disorders including angiogenic ocular disease, ocular inflammation, diabetic retinopathy, corneal graft rejection, glaucoma, ocular edema, cataracts, conjunctivitis and sickle cell retinopathy [75]. In human retinal pigment epithelial ARPE-19 cells, proscillaridin was more potent than ouabain in inhibiting the hypoxia- or IGF-1-induced expression of HIF-1α protein. Furthermore, proscillaridin inhibited the hypoxia-induced expressions of angiogenic factors include VEGF, TIMP and angionenin with IC_{50} values of 32.5, 12.9 and 4.5 nM, respectively, and showed the ability to prevent choroidal neovascularization at a concentration of 60 ng/ml in serum [75]. Also, another steroidal HIF inhibitor, compound 25 (**Figure 5**), was patented by Bionaut International [76]. Similar to the other steroidal HIF inhibitors previously claimed, compound 25 inhibited the hypoxia-induced expression of HIF-1α in Panc-1, Caki-1 and A549 cells, and gave 83% inhibition of tumor growth at 15 mg/ml in a Caki-1 cells implanted xenograft nude mouse model [77]. SRI International also claimed a series of bufadienolide derivatives (R is the nitrogen-containing C_{2-6} heterocyclyl group, such as compound 26 in **Figure 5**) as an HIF modulator for treatment of HIF-1-mediated diseases, particularly neoplastic disorders. However, no detailed biological results were provided.

Another patent application from SRI International claimed a series of substituted l, 3, 5 (10)-estratrienes as steroidal anti-angiogenic and anti-HIF compounds for the treatment of cancer, corneal graft neovascularization, diabetic retinopathy, psoriasis and rheumatoid arthritis [78]. SR-16388 (citrate salt form of compound 27 in **Figure 5**) potently inhibited the hypoxia-induced expression of HIF-1α protein in human prostate cancer PC-3 cells and human breast cancer MDA-MB-231 cells, but did not affect normal cell lines, RAW264.7 macrophages. Additionally, the specific data of anti-angiogenic activity were provided for SR-16388. Among the claimed substituted l, 3, 5 (10)-estratrienes, SR-16388 most potently inhibited the proliferation of human dermal microvascular endothelial cells and the IC_{50} value was about 80 nM. Wound healing experiment showed that a dose of 3 – 30 mg/kg SR-16388 potently inhibited the formation of granulation tissue and resulted in a 30% decrease in microvessel formation as compared to the control group. Furthermore, SR-16388 was active in the inhibition of the proliferation of various types of cancer cells including lung, brain, ovarian, prostate and breast cancers in the range of 0.1 – 1 μM. The results from the PC-3 cells implanted xenograft nude mouse model showed that the oral treatment of 10, 30 and 100 mg/kg SR-16388 markedly reduced tumor growth rates compared to the untreated control group and that microvascularization in the group treated with 30 mg/kg

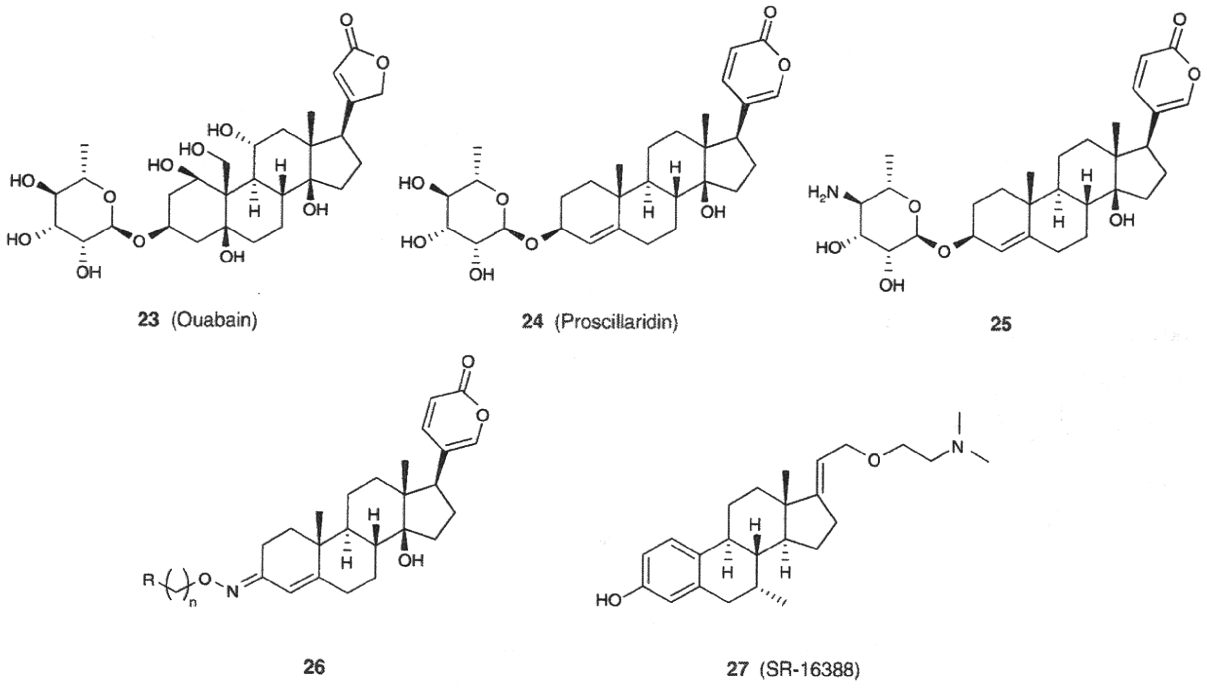

Figure 5. Steroidal HIF inhibitors.

SR-16388 was reduced to about 50% compared to the untreated control group. Furthermore, a combination of SR-16388 at 10 mg/kg and paclitaxel at 7.5 mg/kg produced a much greater inhibition of tumor growth over time. *In vitro* experiments showed that SR-16388 selectively binds to estrogen receptor β (ERβ) with high affinity. Recently, SRI International reported that SR-16388 binds selectively to estrogen-related receptor α (ERRα), but not to ERRβ or ERRγ, and inhibits transcriptional activity of ERRα [79]. However, the relationship between HIF inhibition and ERβ/ERRα inhibition by SR-16388 was not discussed.

4. Peptidic HIF inhibitors

The California Institute of Technology claimed DNA-binding polyamide [80]. The *N*-methylpyrrole and *N*-methylimidazole subunits in polyamide **28** (**Figure 6**) are able to bind to DNA comprising the sequence of 5′-WTWCGW-3′, wherein W is A or T, and the fluorophore (fluorescein isothiocyanate) in the tail of polyamide **28** is able to show its intracellular localization. The interaction of polyamide **28** and HRE (5′-TACGTG-3′) reduces the binding of HIF to HRE, thereby, inhibiting the expression of HIF-inducible genes that include VEGF, VEGF receptor-1 (FIt-1), endothelin-1, endothelin-2, endothelin-3, NOS-2, heme oxygenase-1, EPO, ceruloplasmin, transferrin, transferrin receptor, IGF-binding protein-1, -2 and -3, IGF-II, TGF-B3, COX-1, aldolase A and C, phosphoglycerate kinase-1, phosphofructokinase, glucose transporters 1 and 3, hexokinase 1 and 2, glyceraldehyde-3-phosphate dehydrogenase, enolase 1, pyruvate kinase M, lactate dehydrogenase A and adenylate kinase 3. The activity of polyamide **28** in inhibiting HIF was determined in human cervical carcinoma HeLa cells. VEGF-luciferase reporter gene assay revealed that polyamide **28** inhibited the hypoxia-induced transcriptional activity of HIF in a concentration-dependent manner, and polyamide **28** reduced the iron-chelator desferrioxamine-induced expression of VEGF mRNA and secretion of VEGF protein at concentrations of 0.2 and 1 μM. In addition, real-time quantitative RT-PCR analysis showed that treatment of polyamide **28** for 48 h reduced the level of VEGF expression in a concentration-dependent manner and that ~ 60% of VEGF expression was inhibited by polyamide **28** at 1 μM.

Another patent application from Aileron Therapeutics claimed a series of peptidomimetic macrocycles as peptidic HIF inhibitors [81]. These novel peptidomimetic macrocycle compounds were designed for modulating the activity of HIF-1α through antagonization of the interaction between HIF-1α and p300–CBP transcriptional co-activators. The CAD of HIF-1α contains a region involving p300–CBP interaction. Among the highly conserved α-helices in the region, residue 796 – 805 (TSYDCEVNAP) and residue 814 – 823 (QGEELLRALD) are places that are mimicked by peptidomimetic macrocycles, such as compounds **29** and **30** (**Figure 6**). However, biological or pharmaceutical data for the claimed peptidomimetic macrocycles were not mentioned.